Engineering 29 (2023) 83–94

Contents lists available at ScienceDirect

Engineering

journal homepage: www.elsevier.com/locate/eng

Research
Medical Engineering—Article

Oxygen Penetration Through Full-Thickness Skin by Oxygen-Releasing Sutures for Skin Graft Transplantation

Wenjing Zai [a,c,#], Yunong Yuan [b,#], Lin Kang [a,f,#], Jialong Xu [a], Yiqiao Hu [a], Lifeng Kang [b], Jinhui Wu [a,d,e,*]

[a] State Key Laboratory of Pharmaceutical Biotechnology, Medical School, Nanjing University, Nanjing 210093, China
[b] School of Pharmacy, Faculty of Medicine and Health, University of Sydney, Sydney, NSW 2006, Australia
[c] School of Biomedical Engineering, Shanghai Jiao Tong University, Shanghai 200240, China
[d] Chemistry and Biomedicine Innovation Center, Nanjing University, Nanjing 210023, China
[e] Jiangsu Provincial Key Laboratory for Nano Technology, Nanjing University, Nanjing 210093, China
[f] Jiangsu Food & Pharmaceutical Science College, Huai'an 223003, China

ARTICLE INFO

Article history:
Received 28 January 2023
Revised 11 April 2023
Accepted 6 May 2023
Available online 29 May 2023

Keywords:
Wound
Skin graft transplantation
Oxygen-releasing sutures
Full-thickness oxygen delivery

ABSTRACT

The transplantation of full-thickness skin grafts (FTSGs) is important for reconstructing skin barrier and promoting wound healing. Sufficient oxygen supply is closely related to the success of skin grafting. However, full-thickness oxygen delivery is limited by the poor oxygen permeability of skin. Oxygen-releasing sutures (O_2 sutures) were developed to facilitate oxygen penetration through full-thickness skin. The O_2 sutures delivered 100 times more oxygen than topical gaseous oxygen therapy at a 15 mm depth in the skin model. Under extreme hypoxia (< 0.5% O_2, v/v), O_2 sutures could also promote endothelial cell proliferation. After the transplantation of FTSGs in mice, O_2 sutures accelerated blood re-perfusion and increased the survival area of the skin graft. It is expected that O_2 sutures will be adopted in clinical applications to increase the success rate of full-thickness skin transplantation.

1. Introduction

Skin graft transplantation involves the transplantation of skin from a healthy site to a wound site to promote wound healing [1]; it has significant value in the treatment of surgical incisions including abdominal wall defects and hernias [2–4], thermal burns [5,6], and chronic ulcers [1]. Full-thickness skin grafts (FTSGs) exhibit numerous advantages over split-thickness skin grafts and have an important role in exposed wounds [7,8]. However, the success rate of FTFGs is severely restricted by the local oxygen concentration in the wound tissue, as anoxia (< 0.5% O_2, v/v) leads to cell death [9–11]. Local oxygen concentration depends on the speed of revascularization, which can take 1–2 d post operation [12,13]. Additional oxygen supply immediately after an FTSG procedure can effectively improve graft survival and increase the success of the skin grafting.

To increase the supply of oxygen to wound tissue, several approaches can be applied; these are based on either of two principles: inhalation of gaseous oxygen via the airway and topical delivery of oxygen to the wound tissue [14,15]. After patients breathe 100% oxygen at normal or higher pressures, oxygen can be delivered to the wound site via blood circulation. However, because blood microcirculation requires 1–2 d to reconstruct post-operative FTSGs, oxygen delivery is limited and insufficient for cell proliferation [12,16,17].

To overcome delayed revascularization, oxygen can be delivered topically using either topical gaseous oxygen (TGO) therapy or an oxygen dressing. During TGO therapy, the wound site is directly exposed to 100% gaseous oxygen. Gaseous oxygen first dissolves in the moisture in the epidermis and then diffuses into the skin graft [18–20]. Oxygen dressing is another strategy for topically delivering oxygen to wounds, where dissolved oxygen is produced by peroxide or photosynthetic microbes and then diffuses into the epidermis [21–23]. However, epidermis is virtually impermeable to oxygen and the maximal diffusion distance of oxygen in dermis is between 300 and 700 μm, which is considerably less than the 2–4 mm that FTSGs require [15,24,25]. Therefore, there is an urgent requirement to devise a new approach to effectively deliver oxygen for wound healing after skin graft transplantation. Surgical sutures could be useful in these cases.

* Corresponding author.
E-mail address: wuj@nju.edu.cn (J. Wu).
# These authors contributed equally to this work.

https://doi.org/10.1016/j.eng.2023.05.006

Sutures are surgical threads commonly used to hold body tissues together and approximate wound edges after injury, including FTSG operations. Recent progress in materials and fabrication techniques has enabled the development of a variety of sutures with added functions including monitoring deep wounds [26], antibacterial [27] and anti-inflammatory properties, and wound healing promotion [28]. The added functions capitalize on the fact that sutures are pervious and intimately integrated into the wound tissue upon application. This inspired us to develop a functionalized suture to enhance oxygen delivery to deep skin layers.

In this study, we construct oxygen-releasing sutures (O_2 sutures) for *in-situ* wound oxygen production to promote the success of FTSGs (Fig. 1). The sutures are made from a double-layer hydrogel containing CaO_2 and catalase (CAT). The inner layer of CaO_2 reacts with water to produce H_2O_2; then, the H_2O_2 diffuses to the outer layer and reacts with the CAT to produce oxygen. When used in FTSG operations, O_2 sutures promote the proliferation of endothelial cells in an anoxic environment and accelerate the restoration of blood perfusion of the graft, thereby increasing the success rate of the FTSGs.

2. Materials and methods

2.1. Animal experiments

All animal experiments were performed in compliance with guidelines approved by the Institutional Animal Care and Use Committee of Nanjing University. BALB/c and C57BL/6 mice were purchased from Yangzhou University (China). Human umbilical vein endothelial cells (HUVECs) were purchased from American Type Culture Collection (ATCC).

2.2. Fabrication of O_2 suture

An O_2 suture was fabricated using a double-layer hydrogel wrapping method based on commercial silk sutures. A 4# silk suture (Changchun Shiji Bairuida Pharmacy Co., Ltd., China) was inserted into a conical die with holes at both ends and 8% (w/v) sodium alginate solution (pH 6.7; Sinopharm Chemical Reagent Co., Ltd., China) containing 30 $mg \cdot mL^{-1}$ CaO_2 (China Pharmaceutical Group Chemical Reagents Company Ltd.) was added to the die. The silk core was then pulled from the small hole and immersed in 3% (w/v) calcium chloride solution (pH 7.1; China Pharmaceutical Group Chemical Reagents Company Ltd.) to form an outer CaO_2 hydrogel sheath. Subsequently, the CaO_2 modified suture was inserted into another conical die with sodium alginate solution containing 4.5 $mg \cdot mL^{-1}$ CAT (Beyotime Biotechnology, China) and coated with a CAT hydrogel layer using the previous treatment. CaO_2, CAT, and calcium alginate hydrogel (Alg) sutures were constructed using the same method, however with different hydrogels. The fabrication was performed at room temperature. Sutures were used immediately after they were fabricated; they could be stored at 4 °C by wrapping in plastic wrap and using within 24 h in a special situation.

2.3. Fluorescence labeling of double-layer structure

The double-layer structure of the O_2 suture was labeled with rhodamine B and 123 poly(lactic-*co*-glycolic acid) (PLGA) nanoparticles. The nanoparticles were fabricated using a double emulsion (water/oil/water) solvent evaporation process, as described in our previous study [29]. The nanoparticles were centrifuged at 8000 revolutions per minute (rpm) for 40 min to remove the free dyes. These two fluorescent nanoparticles were mixed in sodium alginate solution and wrapped with silk sutures. The fabricated fluorescence-labeling sutures were embedded in an optimal cutting temperature compound for frozen sections and observed under a fluorescence microscope (FV3000; Olympus Corporation, Japan).

2.4. Suture–sheath bonding test

The bonding between the suture and sheath was tested as previously described [30]. A blank suture was embedded in CaO_2 containing hydrogel. Subsequently, the hydrogel was fixed and the suture was pulled out using a universal tensile-testing machine (68SC-2; Instron, USA). The force and pullout distances were recorded. The adhesion energy between the blank suture and CaO_2 sheath was calculated based on a published equation. The adhesion energy between the blank suture and Alg sheath, and that between the CaO_2 suture and CAT sheath, were calculated using the same method.

2.5. Mechanical characterization of sutures

Suture strength was investigated using the universal tensile-testing machine. Tension strength was determined by the maximal force that the sutures could bear.

2.6. Oxygen-releasing effect of O_2 suture in vitro

The O_2 suture was immersed in phosphate-buffered saline (PBS) (pH 7.4) and the oxygen generation effect of the suture was detected using an oxygen microelectrode (OX-N; Unisence, Denmark). At 6 and 24 h post reaction, the suture was removed from the previous solution and fresh PBS was added to evaluate the continuous oxygen-releasing effect.

The experimental fitting algorithm of the O_2 generating curve was used with Origin Pro 2022 software (v9.9.0.225).

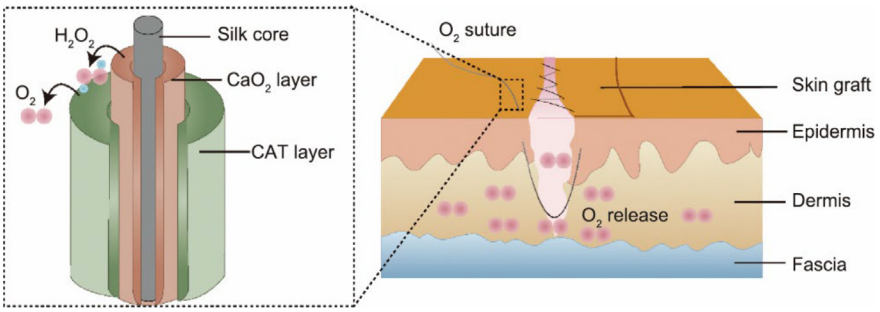

Fig. 1. Schematic of O_2 suture and mechanism to deliver oxygen in skin. CAT: catalase.

2.7. The gelatin hydrogel construction

The gelatin solution (30% w/v) was prepared by water bath at 50 °C for 30 min. The solution was then added to an open plastic pipe (diameter: 13 mm, length: 40 mm) to a height of 20 mm. The solution was held at 4 °C overnight to form the gelatin hydrogel.

2.8. Determination of oxygen transmission efficiency

The oxygen transmission of the porcine skin and gelatin hydrogel at different depths was calculated in a device composed of large and small beakers (volume: 200 and 50 mL). The large beaker was covered with parafilm and filled with pure oxygen to maintain a near-saturated oxygen atmosphere (oxygen flow rate: 1 L·min^{-1} for 1 min and then continuously at 30 mL·min^{-1}). The small beaker was placed inside the large beaker and sealed with parafilm. The gelatin hydrogel containing the plastic pipe or plastic pipe covered with porcine skin was inserted through the parafilm to ensure that oxygen could only enter the small beaker through the gelatin hydrogel or skin. The oxygen electrode was inserted into the small beaker to monitor the oxygen curves inside the small beaker.

2.9. Oxygen penetration in gelatin hydrogel tested by oxygen microelectrode

The oxygen penetration effects of the O_2 sutures and TGO therapy were monitored using the oxygen microelectrode. O_2 sutures were inserted into the center of the gelatin hydrogel and the oxygen curves at different sites were detected by inserting an oxygen microelectrode into different sites. For the TGO therapy test, the gelatin hydrogel was placed in a 200 mL beaker and the oxygen microelectrode was inserted at different sites in the gelatin hydrogel. Pure oxygen was continuously added to the beaker to maintain a nearly maturated oxygen atmosphere. The oxygen curves in the gelatin hydrogel after the TGO therapy were monitored using an oxygen electrode.

2.10. Fick's law with domain discretization

To predict time-dependent oxygen diffusion in the gelatin hydrogel, a two-dimensional model was proposed. In the proposed model, Fick's second law was combined with domain discretization to predict the oxygen evolution of the O_2 suture and TGO system in the gelatin hydrogel. The two-dimensional model represented the central cross-section of the gelatin hydrogel. Owing to the symmetry of the system, half of the entire construction was simulated to conserve computational time and resources. Four hypotheses were assumed in the proposed two-dimensional model to simplify the problems of time and space.

(1) The gelatin hydrogel was assumed incompressible. Gelatin hydrogels are considered nondegradable during oxygen permeation. In addition, the effect of the compression force resulting from the airflow and oxygen probe insertion was neglected.

(2) The oxygen creation rate was assumed to be consistent and uniform in a unit length of the O_2 suture, and the oxygen concentration in each meshed element was assumed to be uniform and perpendicular to the cross-sectional direction. The diffusion of oxygen was assumed to occur only in the *x*- and *y*-directions.

(3) The diffusion coefficient was assumed to be constant throughout the entire gelatin hydrogel, and the effect of oxygen pressure on the diffusion coefficient to be neglectable.

(4) The side and bottom edges were wrapped using a sealed film, and it was assumed that no oxygen exchange occurred at these interfaces. Oxygen exchange with the surroundings occurred only at the top edge of both the suture and TGO systems.

In the proposed model, the oxygen concentration evolution was calculated as follows:

$$\frac{\partial C_{i,j}^{t+\Delta t}}{\partial t} = D \cdot \left(\frac{\partial^2 C_{i,j}^{t}}{\partial x^2} + \frac{\partial^2 C_{i,j}^{t}}{\partial y^2} \right) \tag{1}$$

where t is the time, Δt is the time step, $C_{i,j}^{t}$ is the concentration of the oxygen in the i, j position at time t, and D is the oxygen diffusion coefficient in the gelatin hydrogel. In Eq. (1), the left part represents the oxygen exchange of that element at time t; the right part represents the oxygen exchange with its neighboring elements. The Taylor formula was used to solve this equation.

$$\frac{C_{i,j}^{t+\Delta t} - C_{i,j}^{t}}{\Delta t} = D \cdot \left(\frac{C_{i+1,j}^{t} + C_{i-1,j}^{t} - 2C_{i,j}^{t}}{\mathrm{d}x^2} + \frac{C_{i,j+1}^{t} + C_{i,j-1}^{t} - 2C_{i,j}^{t}}{\mathrm{d}y^2} \right) \tag{2}$$

Because the O_2 suture and TGO system were enclosed by a sealed film, the left and right edges were fixed in the model. Therefore, there were five types of boundary conditions: corner, bottom corner, edge, bottom edge, and internal elements, as indicated in Fig. S1 in Appendix A. For example, the internal elements could exchange oxygen with the top, bottom, left, and right elements. The entire meshed element was updated at each calculation time step. Both proposed models were coded using C in Visual Studio 2022 (v17.0.6).

2.11. Live/dead tests of HUVECs (adherent HUVECs and HUVECs in three-dimensional (3D) hydrogel)

HUVECs were cultured in a 1640 medium supplemented with 10% fetal bovine serum (FBS) and 1% penicillin/streptomycin at 37 °C with 5% CO_2.

For the adherent HUVECs test, the HUVECs were seeded in 24-well plates at a density of 150 000 cells·well^{-1}. After attachment, the cells were divided into seven groups: normoxia (21% O_2), hypoxia (2% O_2), anoxia (< 0.5% O_2; blank), anoxia + O_2 suture, anoxia + TGO, anoxia + CaO_2 suture, and anoxia + CAT suture. Different sutures were co-cultured with the HUVECs on the transwell inserts with 8 μm pore-sized filters. For the anoxia + TGO group, the HUVECs were cultured in pure oxygen for 30 min and then cultured in the anoxic chamber (5% CO_2, < 0.5% O_2) at 37 °C. For the hypxia group, the HUVECs were cultured in the hypoxic chamber (5% CO_2, 2% O_2) at 37 °C. These treatments were repeated 24 h after the initial treatment. The HUVECs were stained with calcein-acetoxymethyl ester (AM) (live) and propidium iodide (dead) to evaluate the live/dead status 48 h after the first treatment.

For the HUVECs in 3D hydrogel, a 2% (w/v) sodium alginate solution was sterilized and mixed with a 1640 medium, FBS, and penicillin/streptomycin after cooling to 42 °C. HUVECs were added to the prepared sodium alginate solution at a density of 300 000 cells·mL^{-1}. HUVEC-sodium alginate solution (1 mL) was added to a confocal cell culture dish (20 mm) and solidified with 250 μL 2% $CaCl_2$ solution to form a 3D hydrogel. The cells were divided into four groups: normoxic, anoxic, anoxic + O_2 suture, and anoxic + TGO. The sutures were embedded in the center of the hydrogel. The HUVECs were stained with calcein-AM (live) and propidium iodide (dead) to evaluate the live/dead status 24 h after treatment.

2.12. Proliferation of HUVECs

HUVECs were cultured in 1640 medium supplemented with 10% FBS and 1% penicillin/streptomycin at 37 °C with 5% CO_2. The cells were seeded into 24-well plates at a density of 50 000 cells·well^{-1}. After attachment, the cell viability was evaluated using a cell counting kit-8 (CCK-8) test. The cells were then divided

into seven groups, similar to those used in the live/dead test for adherent HUVECs. This treatment was repeated 24 h later. Cell viability was evaluated using the CCK-8 test again 48 h after the first treatment. HUVEC proliferation were analyzed by comparing the CCK-8 results on days 0 and 2.

2.13. Autologous skin graft transplantation

Autologous skin graft transplantation was performed on the backs of mice (BALB/c or C57BL/6). A rectangle of skin (1 cm × 2 cm) was cut on three edges (with one short edge connected), lifted to disconnect the blood supply, and carefully sutured. For graft survival research, the mice were randomly divided into six groups: blank suture, O_2 suture, TGO, alginate suture, CaO_2 suture, and CAT suture. Typically, we sewed approximately ten stitches per flap. For the TGO group, grafts received pure oxygen at a flow of 0.25 $L{\cdot}min^{-1}$ for 30 min. Images of the transplanted grafts were obtained daily. On days 3 and 6, the mice were euthanized and grafts were collected for further research. For blood perfusion and angiogenesis studies, the mice were randomly divided into four groups: blank suture, O_2 suture, TGO, and alginate. Blood flow was detected using a MoorFLPI (Moor Instruments, UK).

2.14. Histology and immunohistochemistry

Mice were euthanized three or six days post treatment and the skin grafts were embedded in paraffin. Paraffin-embedded tissue was used for the immunohistochemical analysis. Slices of the graft were observed on day 6 using hematoxylin and eosin staining. Graft slices on day 3 were observed using Masson's staining and cluster of differentiation 31 (CD31) incubation. For CD31 incubation, slices were dehydrated and incubated with 3% H_2O_2 to block endogenous peroxidases. After antigen retrieval and blocked with serum, the slices were incubated with anti-CD31 antibody at 4 °C overnight and then incubated with horseradish peroxidase-conjugated secondary goat anti-rat antibody at room temperature for 30 min. Sections were observed and photographed using a microscope connected to a digital camera.

2.15. Statistical analysis

The statistical significance was determined using unpaired and paired two-sided student's *t*-tests for two groups and one-way analysis of variance (ANOVA) for more than three groups; data were presented as single measurements with bars as means ± standard error (SE). Statistically significant *P* values are indicated in the figures and/or legends as $^{****}P < 0.0001$, $^{***}P < 0.001$, $^{**}P < 0.01$, and $^{*}P < 0.05$. NSD indicated no significant differences.

2.16. Data availability

All data supporting the findings of this study are available within the article and Appendix A and from the corresponding author upon reasonable request.

3. Results

3.1. Fabrication and characterization of O_2 sutures

We constructed O_2 sutures through a double-layer wrapping method with commercially available surgical silk sutures. Specifically, we inserted the silk thread core into a conical die with holes at both ends and added a sodium alginate solution containing CaO_2 to the die. The silk core was then removed from the small hole and immersed in a calcium chloride solution to form an outer CaO_2 hydrogel sheath. Subsequently, the CaO_2-modified suture was inserted into another conical die with a sodium alginate solution containing CAT and coated with a CAT hydrogel layer with the previous treatment (Fig. 2(a)). The sutures were verified using a continuous-zoom stereomicroscope. The diameter of the O_2 suture was approximately 0.4 mm, and the hydrogel shell was evenly wrapped around the suture. The O_2 sutures were bent and knotted freely after being wrapped with the hydrogel; the knotting step did not impair the hydrogel on the surface of the O_2 sutures (Fig. 2(b)). The double-layered structure around the suture core was further confirmed by fluorescence labeling (Fig. 2(c)).

Strong bonding between the suture core and sheath is critical to guarantee the integrity of an O_2 suture during surgery. The strong bonding ensures that the hydrogel sheath does not easily fall off the suture surface during surgery. To quantify the bonding between the suture and hydrogel sheath, a pullout test was designed. The sutures were embedded in the hydrogel and pulled out using a universal tensile-testing machine. Both the forces and pullout distances were recorded to quantify the bonding (Fig. 2(d)). The adhesion energy was calculated using a previously published method [30]. The adhesion energy between the silk suture core and CaO_2 hydrogel and that between the CaO_2 suture and CAT hydrogel both exceeded 1000 $J{\cdot}m^{-2}$ (Fig. 2(e)), indicating strong bonding among all ingredients and excellent O_2 suture integrity.

We further investigated the O_2 suture tensile strength using a universal tensile-testing machine. The curves of the force change with stretching distance are displayed in Fig. S2 in Appendix A. The O_2 sutures achieved a maximum tension of 10 N, which was approximately 1.5 N greater than that of blank sutures (Fig. 2(f)). This could be because the outer sheath helped to maintain the integrity of the sutures. The multifilament sutures were united and jointly counteracted the pulling force, thus exhibiting superior maximum tension.

To detect the oxygen generation, O_2 sutures were immersed in PBS (Fig. 2(g)). The O_2 sutures generated O_2 rapidly after being immersed in the PBS, and the O_2 concentration increased from 280 to approximately 900 $\mu mol{\cdot}L^{-1}$ (approaching the saturation of dissolved oxygen) in 2 h. The sutures were removed from the original PBS and reimmersed in fresh PBS. It was found that the O_2 sutures generated oxygen for more than 24 h. In addition, a large number of small bubbles were observed around the sutures after 10 min of immersion, and the sutures floated after 2 h of immersion (Fig. 2(h)), likely owing to the buoyancy provided by the large number of generated oxygen bubbles. The O_2 sutures swelled during water absorption and oxygen production. The diameter of the swollen sutures was approximately 0.8 mm. The O_2 sutures maintained similar oxygen producing ability for 24 h after storage at 4 °C (Fig. S3 in Appendix A).

O_2 sutures were fabricated through double-layer wrapping of the CaO_2- and CAT-containing hydrogels. CAT in the outer layer catalyzes H_2O_2 relieved from the inner layer to provide O_2 and avoids H_2O_2 release. The H_2O_2 release content of the O_2 sutures was maintained at zero in solution. The sutures modified with CaO_2 containing hydrogel released a large amount of H_2O_2 (Fig. S4 in Appendix A). The double-layer wrapping design can prevent cell damage due to the potential oxidative stress caused by H_2O_2.

3.2. Oxygen penetration capability of O_2 sutures

We used a gelatin hydrogel to simulate skin to investigate the oxygen penetration capability of the O_2 sutures. Gelatin is the product of the partial hydrolysis of collagen, which is the main component of skin. A device for measuring the oxygen diffusion was developed (Figs. S5(a)–(c) in Appendix A). The device consisted of internal and external containers. The oxygen concentration in the

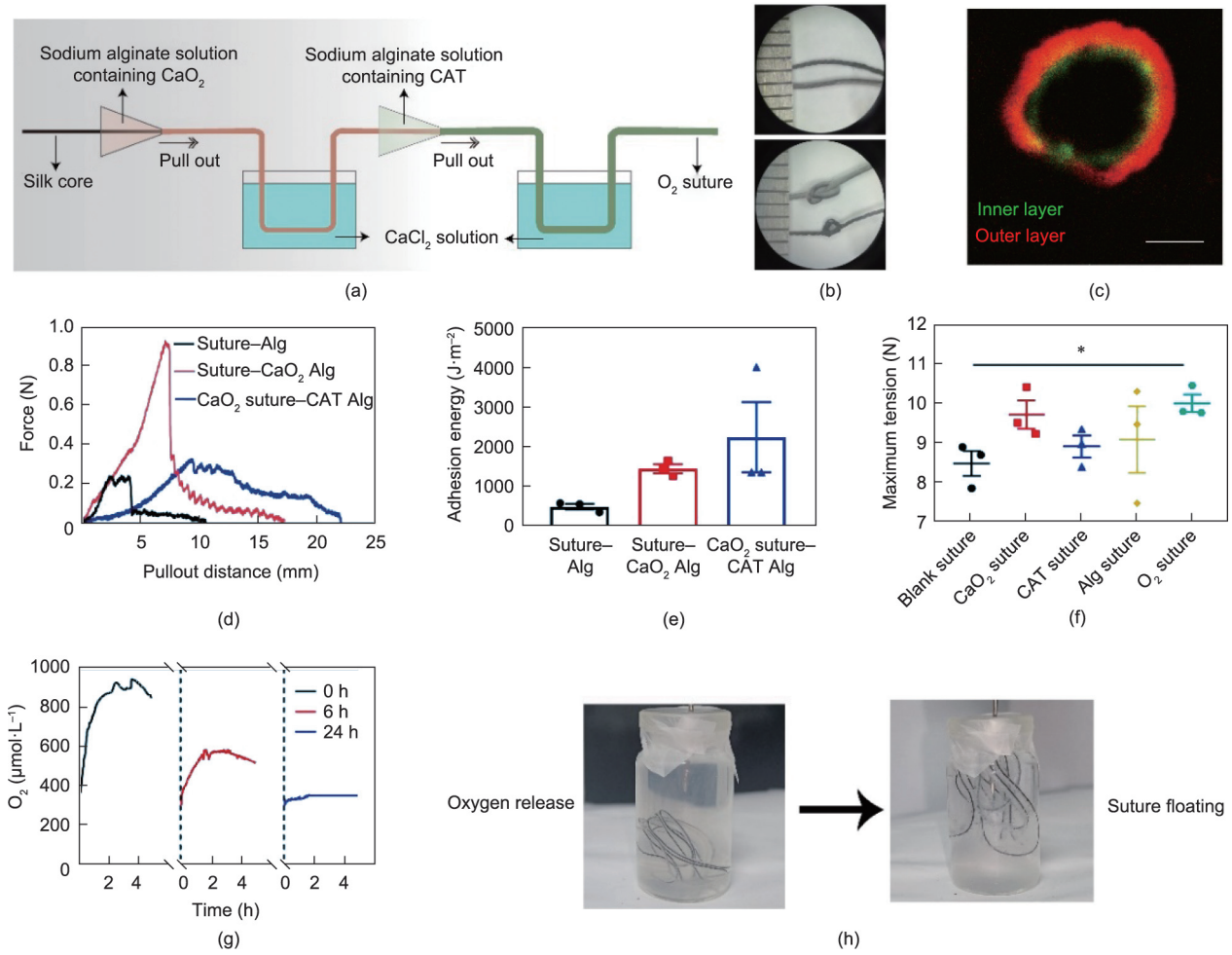

Fig. 2. Fabrication and characterization of O_2 sutures. (a) Schematic of fabrication of O_2 sutures. Hydrogel sheath containing CaO_2 and that containing CAT are in turn coated onto a silk suture core. (b) Microscopic images of blank sutures and O_2 sutures. Upper: unfolded sutures; lower: folded sutures. Minimum scale of ruler is 1 mm. (c) Fluorescence labeling of two-layer sheath of CAT–CaO_2 sutures. Scale bar: 150 μm. (d) Representative force–displacement curves between sutures and hydrogel sheaths tested by pullout tests. Suture represents blank silk suture and CaO_2 suture represents silk suture coated with Alg containing CaO_2 (CaO_2 Alg). (e) Adhesion energy between different sutures and hydrogel sheaths calculated from pullout tests in (d). (f) Maximum tension of sutures with different modification tested by tensile tests. (g) Oxygen production curves of O_2 suture. O_2 suture was taken from original solution and added to fresh PBS at different time points to investigate its long-term oxygen generating effect. (h) Representative images of O_2 sutures in PBS. The image on the left is the appearance ten minutes post O_2 suture insertion, there are a large number of bubbles around the sutures. The image on the right is the appearance 2 h post O_2 suture insertion; the sutures are floating upwards.

internal container was used to represent the oxygen penetration of the skin and gelatin hydrogel. After calibration, a gelatin hydrogel with a thickness of 20 mm was used as the optimal model to simulate actual skin (Figs. S5(d) and (e) in Appendix A). TGO therapy was used as a control for comparison with the O_2 sutures.

It was hypothesized that O_2 sutures could provide deeper oxygen penetration than TGO therapy because the O_2 sutures could pass through the skin (Fig. 3(a)). To test this hypothesis, the oxygen penetration was evaluated using a gelatin-hydrogel skin model. The O_2 sutures were inserted into gelatin hydrogel with a thickness of 20 mm and diameter of 13 mm. Different positions in the gelatin hydrogel were defined using x and y, where x represented the horizontal distance from the O_2 suture (or the center of the hydrogel in the TGO group), and y represented the vertical distance from the surface of the gelatin hydrogel. The oxygen concentrations at different positions in the gelatin hydrogel were then tested (Figs. 3(b)–(g)). At 3600 s post insertion, the oxygen concentration at all positions of the O_2 sutures was greater than 50 $\mu mol·L^{-1}$, which was considerably higher than that at the same positions in the TGO control group. In particular, at positions 2 and 3, the oxygen concentration through the O_2 sutures at 3600 s post insertion was greater than 200 $\mu mol·L^{-1}$, which was considerably higher than that in the TGO control group (<10 $\mu mol·L^{-1}$). To further evaluate the oxygen diffusion profile of the O_2 sutures, positions with the same x or y values were compared (Figs. 3(h) and (i)). At positions 2 and 3 (same x value), O_2 sutures delivered 50 and 100 times more O_2 than the TGO therapy, respectively. At positions 3, 6, and 7 (same y value), the O_2 sutures delivered 100 times more O_2 than the TGO therapy. These results indicate that O_2 sutures can achieve full-thickness delivery of oxygen to the skin. In particular, O_2 sutures can promote oxygen penetration deeper into gelatin gels, which is not possible with TGO therapy.

3.3. Computational digital simulation of oxygen penetration of O_2 sutures

To further verify our hypothesis that O_2 sutures can achieve full-thickness oxygen penetration and enhance oxygen delivery efficiency in deep skin layers, we compared oxygen distribution in the gelatin hydrogel using a computational simulation method.

Fick's law of diffusion was combined with the domain discretization model to simulate the spatial and temporal evolution

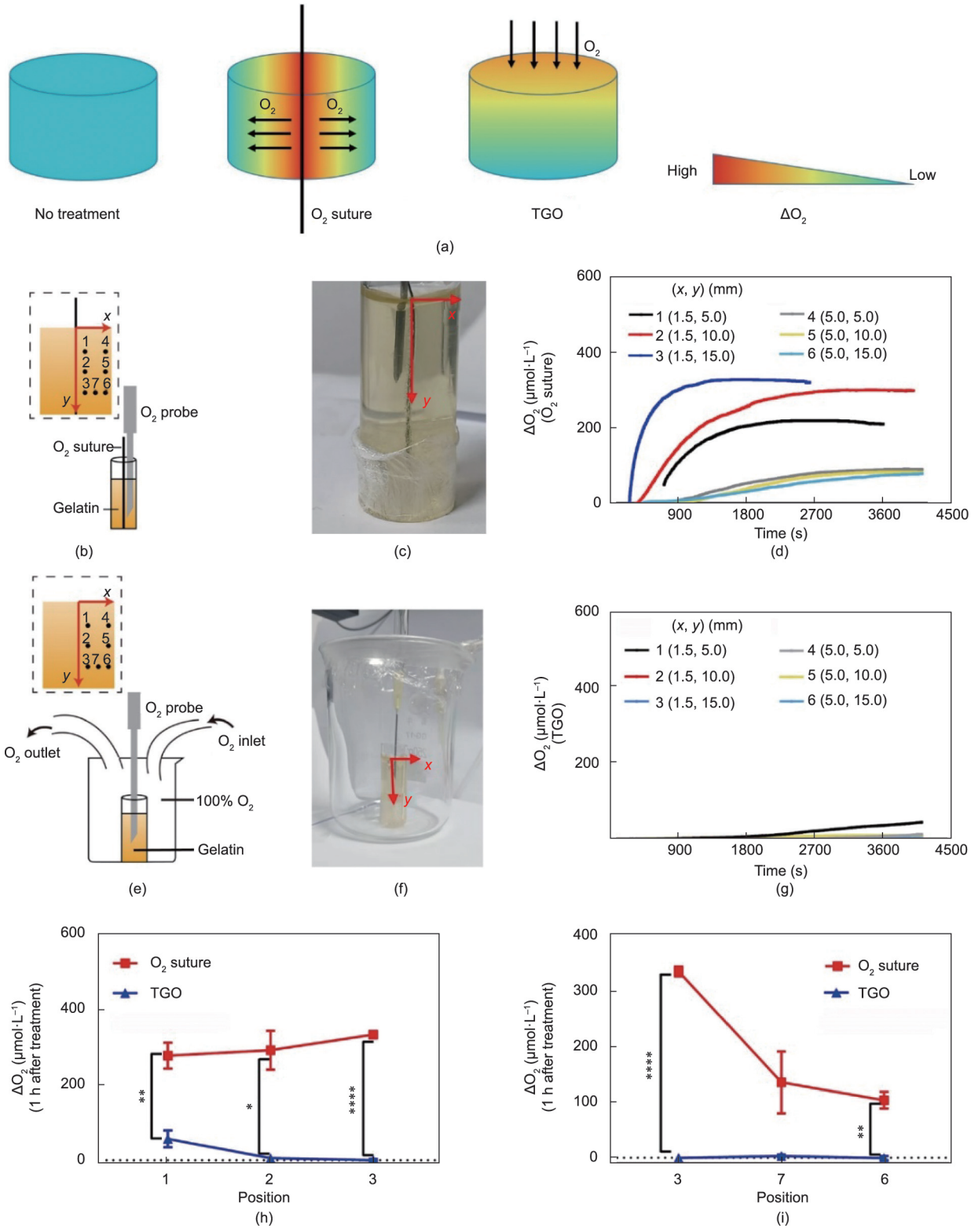

Fig. 3. Comparison of oxygen penetration between O_2 sutures and TGO therapy. (a) Schematic illustration of speculation for oxygen permeability through O_2 suture or TGO therapy in the gelatin hydrogel. (b) Schematic illustration of device to monitor oxygen diffusion through O_2 suture therapy. Oxygen microelectrode was inserted at different positions of the gelatin hydrogel and sutures were inserted in the center of the gelatin hydrogel. Different positions (1, 2, 3, 4, 5, 6, 7) in gelatin hydrogel were defined using *x* and *y*, where *x* represents horizontal distance from O_2 suture and *y* represents vertical distance from gelatin-hydrogel surface. (c) Image of device to monitor oxygen diffusion through O_2 suture therapy. (d) Oxygen concentration curves for O_2 suture therapy at different positions of gelatin hydrogel. (e) Schematic illustration of device to monitor oxygen diffusion through TGO therapy. Gelatin hydrogel was placed in a container that was continuously filled with oxygen. (f) Image of device to monitor oxygen diffusion through TGO therapy. (g) Oxygen concentration curves for TGO therapy at different positions of gelatin hydrogel. (h) Changes of oxygen concentration (ΔO_2) at different depths of the gelatin hydrogel with the same *x* value 1 h post treatment. (i) Changes of oxygen concentration (ΔO_2) at different widths of the gelatin hydrogel with the same *y* value 1 h post treatment. Gelatin hydrogel was used as the simulated skin model. $n = 3$ in (h) and (i).

of the oxygen concentration through O_2 sutures and TGO therapy, respectively (Fig. S1). The parameters used in the proposed model are listed in Table 1 [31]; the rate of O_2 suture-produced oxygen was calculated using Eq. (3). The oxygen production rates of the O_2 sutures and their exponential fitting curves are displayed in Fig. S6 in Appendix A. Representative points in the gelatin hydrogel were selected to validate the proposed model for predicting the evolution of the oxygen concentration (Figs. 4(a)–(c)). The predicted results agreed well with the experimental results obtained using O_2 sutures and TGO therapy, thus validating the reliability of the proposed simulation model.

$$y = -622.51 \cdot \exp\left(-\frac{x}{2387.76}\right) + 597.64 \quad (3)$$

Table 1
The related values of parameters in the proposed model.

Parameters	Values
Gelatin hydrogel depth and width (mm)	H = 20, W = 6.5
Suture length and width (mm)	L_{sut} = 20, W_{sut} = 0.4
Grid size (mm)	dx = 0.1, dy = 0.1
Diffusion coefficient ($m^2 \cdot s^{-1}$)	D = 0.0027 [31]
Convection coefficient ($m \cdot s^{-1}$)	h = 0.005
Time step (s)	Δt = 0.1

After validating the simulation model, the distribution dynamics of released oxygen in the gelatin hydrogel were calculated (Fig. 4(d)). An O_2 suture with a length of 20 mm was inserted into the gelatin hydrogel and compared with TGO therapy. Oxygen in the O_2 suture diffused horizontally, indicating that the concentration of oxygen at positions with the same x value was similar. In the TGO group, oxygen diffused vertically, indicating that the concentrations of oxygen at positions with the same y values were similar. In the O_2 suture group, from 500 to 5000 s, the oxygen concentration increased from 200 to 300 $\mu mol \cdot L^{-1}$ at all positions with x = 1 mm. At 5000 s, the oxygen concentration reached 100 $\mu mol \cdot L^{-1}$ at all positions with x = 5 mm, which is sufficiently high for cell growth and proliferation. In the TGO group, because the oxygen diffused vertically, the concentration of oxygen at positions with y > 10 mm was zero from start to finish. Taken together, these results demonstrate that the O_2 suture had acceptable oxygen perfusion, especially for thick skin tissue.

3.4. Survival and proliferation of anoxic endothelial cells mediated by O_2 sutures

Transplanted tissues experience hypoxia (< 5% O_2, v/v) and anoxia (< 5% O_2, v/v) owing to the poor blood supply and oxygen consumption. Anoxia environments further hamper cell proliferation, cause

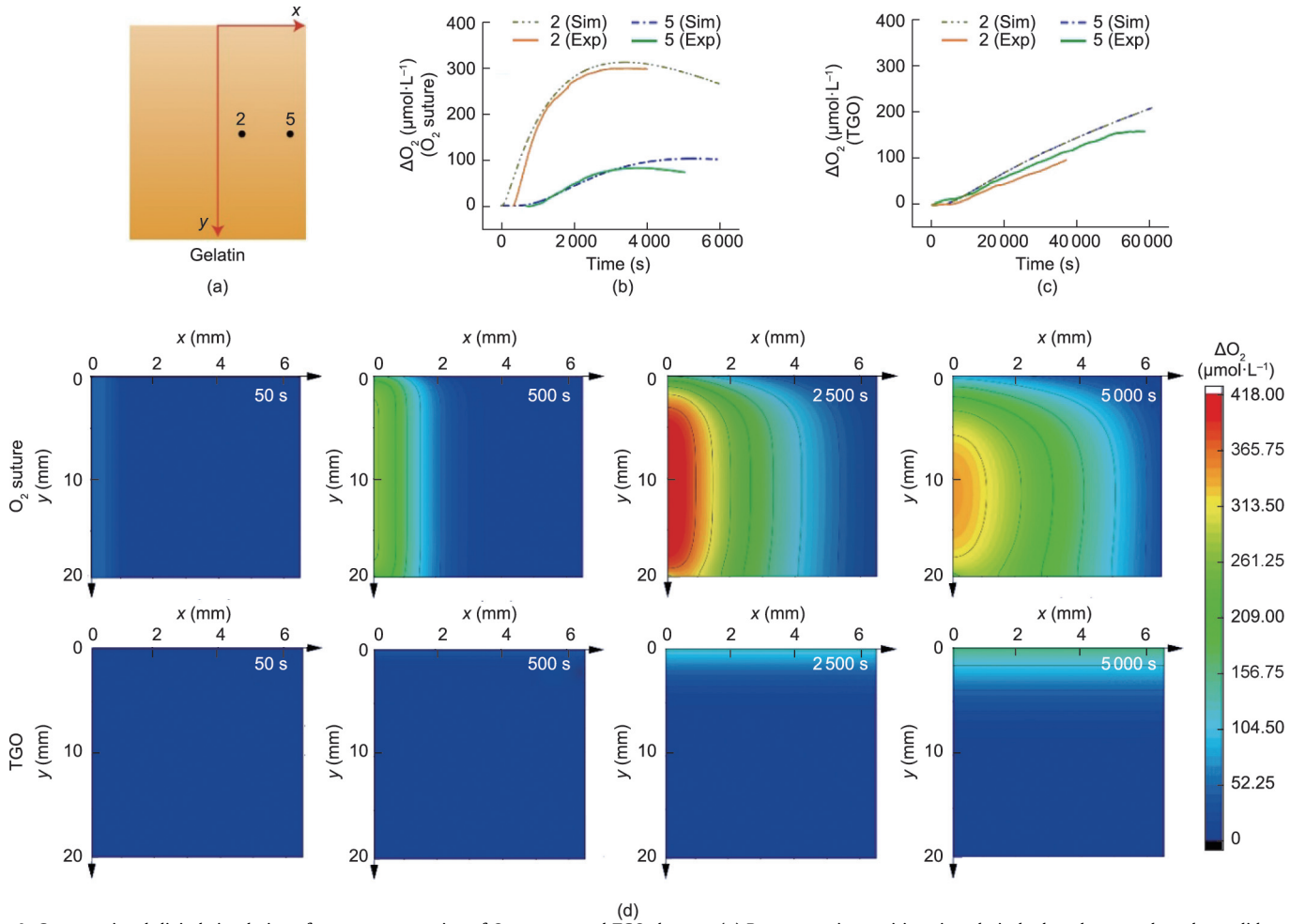

Fig. 4. Computational digital simulation of oxygen penetration of O_2 sutures and TGO therapy. (a) Representative positions in gelatin hydrogel were selected to validate proposed model. Position 2: x = 1.5 mm, y = 10.0 mm; position 5: x = 5.0 mm, y = 10.0 mm. (b) Experimental oxygen curves (Exp) and simulated oxygen curves (Sim) at positions 2 and 5 using O_2 sutures. (c) Experimental oxygen curves (Exp) and simulated oxygen curves (Sim) at positions 2 and 5 using TGO therapy. (d) Simulation results of oxygen distribution in gelatin hydrogel through O_2 sutures (top) and TGO therapy (bottom) varied with time (50, 500, 2500, and 5000 s).

cell death, and limit angiogenesis, both leading to transplantation failure [11,31]. Therefore, we investigated the effects of O_2 sutures on the survival and proliferation of HUVECs under anoxic conditions.

HUVECs were cultured under normoxic, hypoxic, and anoxic conditions. Anoxic HUVECs were divided into different groups and treated with O_2 sutures, CaO_2 sutures, CAT sutures, or TGO therapy separately. Cell survival and death were detected using live/dead tests 48 h after co-culturing (Fig. 5(a)). The HUVEC live/dead rate declined approximately 70% under anoxic conditions, whereas the O_2 suture group maintained cell survival at a live/dead rate similar to that of the normoxic group (Fig. 5(b)). Cell proliferation was also evaluated (Fig. 5(c)). O_2 sutures also promoted HUVEC proliferation under anoxic conditions. To emulate true skin conditions, we seeded HUVECs in 3D hydrogel (2% calcium

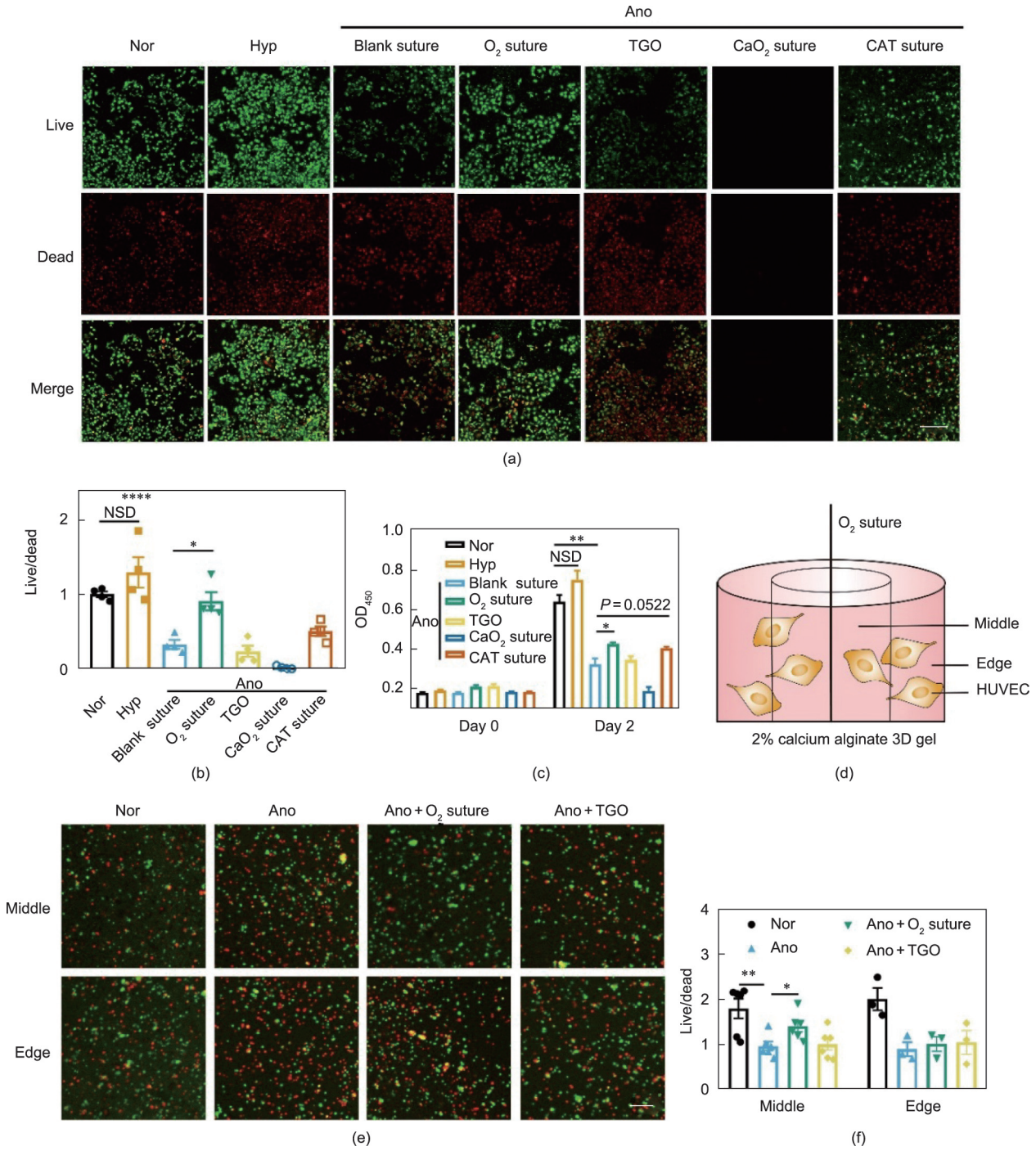

Fig. 5. Promotion of HUVEC survival and proliferation under anoxic conditions induced by O_2 sutures. (a) Representative fluorescent images of adherent HUVECs with different treatments stained with calcein-AM (green, live) and propidium iodide (red, dead). TGO therapy was operated for 0.5 h before culturing cells in anoxia environment. Sutures were put above the trans-well inserts for co-culture with HUVECs. Scale bar: 300 μm. (b) Semi-quantification of relative live/dead rates for HUVECs as displayed in (a). (c) HUVECs proliferation tested by CCK-8 tests. (d) Schematic illustration of HUVECs cultured in 3D hydrogel. O_2 suture was inserted in center. The region with a 5 mm radius around the sutures was considered as the middle and the remaining area was the edge. (e) Representative fluorescent images of HUVECs in 3D hydrogel with different treatments stained with calcein-AM (green, live) and propidium iodide (red, dead). Scale bar: 200 μm. (f) Semi-quantification of live/dead rates for HUVECs as displayed in (e). Nor: normoxia; Hyp: hypoxia; Ano: anoxia; OD_{450}: optical density at 450 nm.

alginate) and inserted O_2 sutures into the hydrogel center (Fig. 5(d)). HUVEC 3D hydrogels were cultured under different O_2 conditions and live/dead rates were detected (Fig. 5(e)). Similar to the case of the adherent cells, the O_2 sutures promoted HUVEC survival in the 3D hydrogels, and the promotion effect was maintained within a radius of 5 mm around the O_2 sutures (Fig. 5(f)).

3.5. Effect of O_2 sutures on the survival, blood perfusion, and angiogenesis of transplanted FTSGs

To investigate whether O_2 sutures could benefit FTSG survival, we evaluated the effects of O_2 sutures in an autologous skin graft transplantation model in BALB/c mice. Rectangular grafts (2 cm long and 1 cm wide) were cut from the backs of the mice, with one short side connected, peeled from the subcutaneous tissue, and sewn with sutures (Fig. 6(a)). The mice were divided into six groups: blank sutures (sewn up with commercial silk sutures), Alg sutures (silk sutures coated with Alg), O_2 sutures, TGO, CaO_2 sutures, and CAT sutures. Owing to the disrupted blood supply and oxygen consumption of the skin grafts from the recipients, the grafts were prone to necrosis, especially at the site distal to the connected edge (Fig. 6(b)). We quantified the necrosis rate of the skin grafts six days after treatment (Fig. 6(c)). The average necrosis rates in blank sutures, Alg sutures, TGO, CaO_2, and CAT sutures were 27.2%, 32.0%, 24.4%, 40.0%, and 30.4%, respectively. Specifically, the necrosis rate in the O_2 suture group declined to

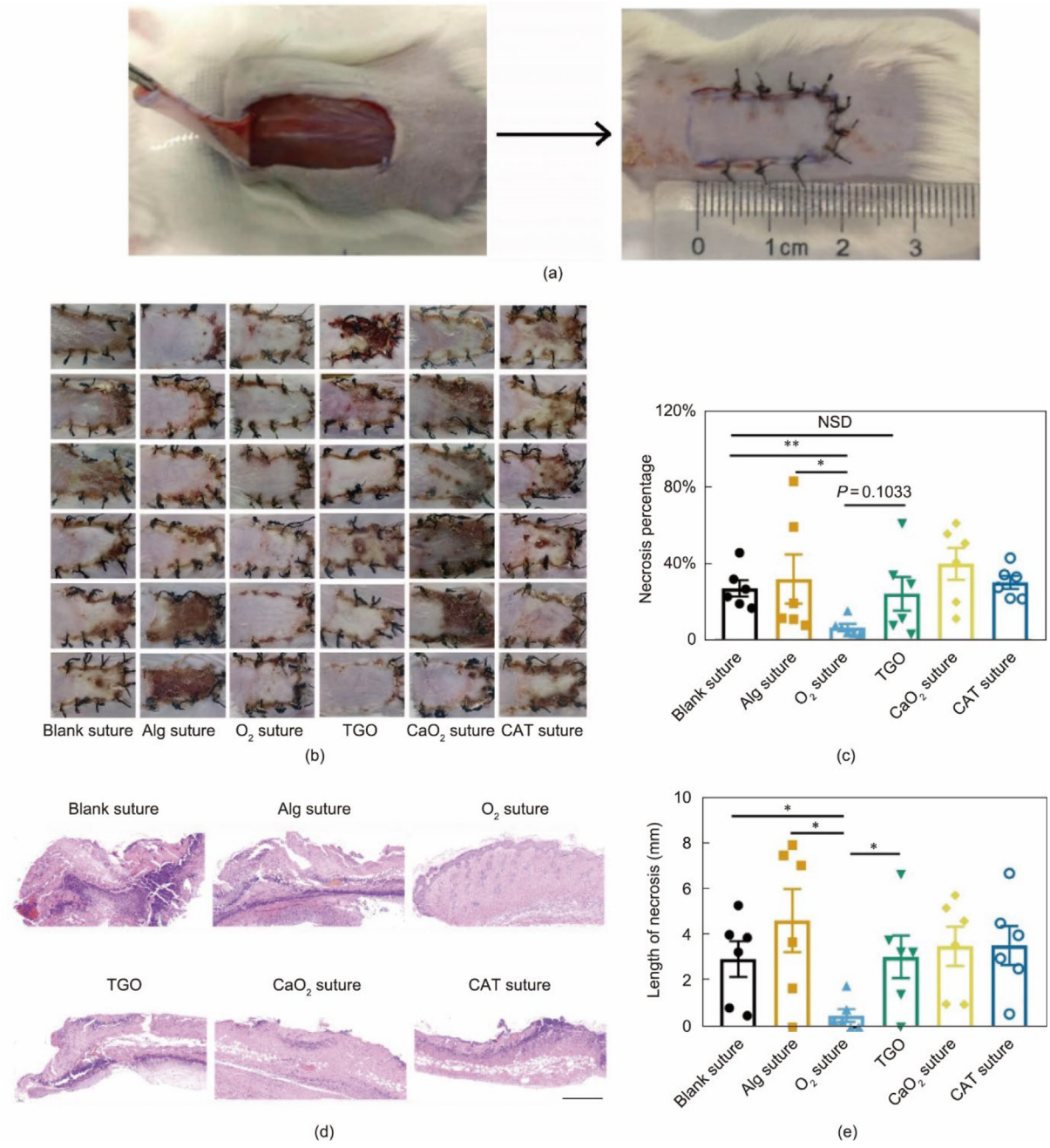

Fig. 6. Transplanted skin graft survival induced by O_2 sutures. (a) Images illustrate progress of autologous skin graft transplantation. (b) Representative images of transplanted skin grafts six days post operation. (c) Quantification of graft necrosis percentage as displayed in (b). (d) Representative hematoxylin and eosin (H&E) images of skin grafts six days later. Scale bar: 500 μm. (e) Quantification of necrosis length of skin graft as displayed in (d), n = 6.

only 6.6%, which was considerably less than other groups. We found that the TGO treatment marginally reduced the necrosis rate, which could have been due to poor oxygen delivery efficiency. The CaO_2 sutures exacerbated necrosis, which could have been due to the oxidative stress caused by the released H_2O_2. The deposition of collagen decreased on day 3, whereas that with O_2 suture treatment was maintained (Fig. S7 in Appendix A). On day 6, the necrotic graft lost its intact epithelial structure, and the number of hair follicles decreased. It was confirmed that the O_2 suture treatment preserved the intact epithelial structure and hair follicles (Fig. 6(d)). Moreover, the O_2 sutures decreased necrosis length, with the average necrosis length of 0.52 mm, which was considerably less than the 2.98 mm in the blank suture group (Fig. 6(e)). This positive role in promoting skin graft survival was further confirmed in C57BL/6 mice (Fig. S8 in Appendix A).

We investigated the blood perfusion of skin grafts daily using laser Doppler flowmetry (Fig. 7(a)). Blood flow was plentiful before the experiment; however, it decreased sharply after the experiment owing to the disruption of blood vessels. In particular, limited blood perfusion was more prominent distant from the connected site of the skin. We divided the skin graft into three regions: proximal (near the connected site), middle, and distal (distant from the connected site) (Fig. 7(b)). The relative blood flux at the middle and distal sites relative to that at the proximal sites was quantified (Figs. 7(c)–(e)). Middle and distal blood fluxes in the blank suture group both decreased for approximately 30% post operation and did not recover over the next six days. TGO therapy improved the blood perfusion of the middle site slowly by approximately 10%; however, it could not increase blood flux at the distal site. Surprisingly, we found that the O_2 suture treatment had a positive effect on blood perfusion at both the middle and distal sites. O_2 sutures lightened the reduction in blood flow at the middle sites one day post treatment and maintained this over next time. For the distal sites, although blood flow decreased one day later, it returned to near normal after two days in the O_2 suture group. These results indicate that O_2 suture treatment improved blood re-perfusion in transplanted skin grafts.

To investigate whether O_2 sutures promoted angiogenesis of skin grafts, we quantified blood vessel densities in the blank suture, O_2 suture, TGO, and Alg suture groups using CD31 immunohistochemical staining at three days post treatment. CD31 is a platelet/endothelial cell adhesion molecule widely used to label endothelial cells and evaluate angiogenesis during wound healing [21]. O_2 suture treatment significantly increased the number of CD31 positive vessels. The average vessel density in the O_2 suture group was 2.4 times of that in the blank suture group, 2.2 times

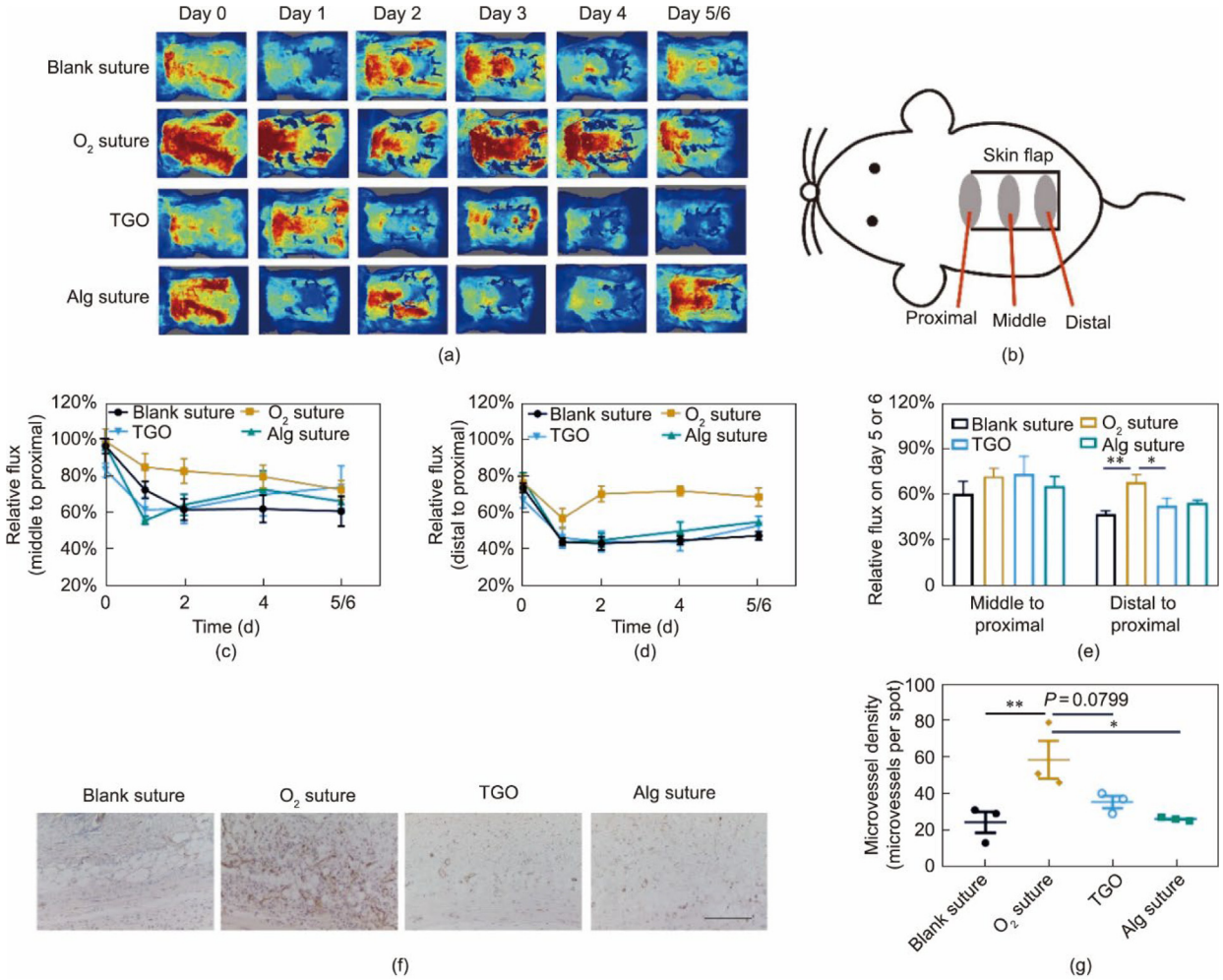

Fig. 7. Re-perfusion and angiogenesis promotion of transplanted skin graft mediated by O_2 sutures. (a) Representative blood flow images captured by laser Doppler flowmetry. (b) Schematic illustration of proximal, middle, and distal sites of skin graft. (c) Curves of relative flux in middle site of grafts. (d) Curves of relative flux in distal site of grafts. (e) Quantification of relative flux five or six days post operation in middle and distal sites. (f) Representative images of CD31 staining three days post operation. Scale bar: 100 μm. (g) Microvessel density of skin grafts three days post operation. In (c)–(e), n = 8 in O_2 suture group, and n = 7 in blank suture, TGO, and Alg suture groups. In (g), n = 3 for each group.

that in the Alg suture group, and 1.6 times that in the TGO group (Figs. 7(f) and (g)). In recent years, the von Willebrand factor (VWF), a hemostatic protein, has been demonstrated to regulate blood vessel formation. The loss of VWF in endothelial cells results in dysfunctional angiogenesis and vascular malformations [33,34]. We investigated VWF expression to evaluate the angiogenesis-promoting effects of the O_2 sutures. The expression of VWF was significantly higher in this group than in the other groups. In particular, VWF expression in the O_2 suture group was 3.9 times that in the blank suture group and twice that in the TGO group (Fig. S9 in Appendix A). These results indicate that O_2 sutures could accelerate angiogenesis after graft transplantation, thus benefiting blood re-perfusion and skin graft survival.

4. Discussion

O_2 sutures were designed to achieve full-thickness oxygen penetration during FTSG transplantation. The oxygen supply in FTSGs is limited by the excessive thickness. It is difficult for new blood vessels to pass through grafts thicker than 0.4 mm quickly and the grafts can suffer from poor oxygen transportation [35]. Thus, FTSG transplantation is restricted by the stringent requirements for an acceptable blood bed [7,36]. Additional oxygen delivery through the skin is important to promote the success of FTSG transplantation, especially for patients in the inferior blood bed group. Existing oxygen delivery strategies such as TGO therapy deliver oxygen from the surface to the deep skin, and their efficiency is hampered by poor oxygen penetration into the skin. O_2 sutures pass through the entire skin layer and remain at the wound site. Unlike existing strategies, they deliver oxygen horizontally throughout the skin. Thus, O_2 sutures can overcome the obstacle of skin thickness and realize full-thickness oxygen delivery, especially by improving oxygen penetration in deep skin.

In particular, O_2 sutures can provide significant benefits in the treatment of abdominal hernias repaired with FTSGs. The recurrence rate of hernia is up to 33% when treated with conventional mesh reinforcement [37]. FTSGs have recently gained attention in large incisional hernia repair. Serious complications in abdominal surgeries, including the incarceration of abdominal contents, impair blood supply, and further limit oxygen delivery [3]. Thus, it is more meaningful to relieve deep anoxia in abdominal FTSGs using O_2 sutures for abdominal hernia repair.

A clinical retrospective study of 1142 free graft procedures indicated that 91% of graft failures occur within a 48 h window, emphasizing the importance of blood perfusion recovery at the early stage of transplantation [35]. Extreme hypoxia (anoxia) inhibits revascularization, which hampers cell metabolism and proliferation [9,10]. The O_2 suture treatment improves endothelial cell survival and promotes endothelial cell proliferation in anoxic environments (Fig. 5). O_2 sutures promoted angiogenesis and blood re-perfusion in the autologous skin graft transplantation models of mice (Fig. 7 and Fig. S9). This is important for skin grafting because it guarantees sustained transport of oxygen and nutrients post transplantation and thus promotes the long-term survival of skin grafts.

Fick's second law combined with domain discretization has been extensively used to predict oxygen or drug diffusion in skin and other tissue [31,38,39]. The proposed 2D oxygen diffusion model using Fick's second law proved effective in predicting the time-dependent oxygen evolution in gel, as evidenced by the successful matching of the experimental results (Figs. 4(b) and (c)). However, the accuracy of the model is somewhat limited owing to the simplified assumptions made in the model, including a constant diffusion coefficient and neglecting the effect of oxygen pressure on the diffusion coefficient. Moreover, the largest deviation observed in the model was less than 19.6 $\mu mol \cdot L^{-1}$ (< 6.3%), which could be due to differences in the oxygen creation rate between the O_2 sutures submerged in PBS and in the gel. Despite these limitations, the proposed model demonstrated promising potential; incorporating more complex factors such as the effect of verifying the diffusion coefficient and oxygen pressure on the diffusion coefficient could improve the model's reliability. In addition, to simulate the entire process in the skin accurately, it is essential to add the oxygen consumption component to the oxygen evolution equation because skin cells consume a portion of oxygen during metabolism while diffusing over distance.

O_2 sutures are expected to realize efficient oxygen delivery along the entire wound edge and induce revascularization between grafts and hosts in clinical applications. We evaluated the maximum oxygen delivery radius of O_2 sutures further to determine the recommended distance between stitches. The effective distance was defined as the point at which the oxygen concentration was greater than 50 $\mu mol \cdot L^{-1}$ in the gelatin hydrogel. As indicated in Fig. S10 in Appendix A, the effective distance for oxygen delivery through the O_2 sutures was approximately 14 mm. Converting to actual skin (3 mm skin being approximately 20 mm gelatin hydrogel), the effective distance was approximately 2.1 mm in the skin. Thus, to ensure sufficient oxygen penetration between the suturing edges, the distance between the stitches should be less than 4.2 mm. In general, the distance between stitches is approximately 5–10 mm in clinical suturing [40]. Thus, the 4.2 mm distances between the stitches of the O_2 sutures would be barely sufficient to ensure oxygenation alongside the wound edge. The O_2 sutures could be further optimized to extend their oxygen delivery distance by optimizing the loaded CaO_2. Moreover, the effect of O_2 sutures on large grafts could be further investigated in the future.

5. Conclusions

We demonstrated that O_2 sutures, which can deliver oxygen deep into the skin, promoted skin graft revascularization and survival. The deep oxygen delivery of the O_2 sutures was examined by combining experimental measurements with a microelectrode and computational digital simulation. O_2 sutures delivered 100 times more oxygen than TGO therapy to the deep skin. Effective oxygen delivery promotes endothelial cell survival and proliferation in anoxic environments. *In vivo* studies demonstrated that O_2 sutures alleviated necrosis in transplanted skin grafts and stimulated angiogenesis and blood re-perfusion, hence improving the success of skin grafting. Our design provides a new approach for deep oxygen delivery in skin grafting, and O_2 sutures should have an excellent possibility to be adopted in clinical applications.

Acknowledgments

This paper was supported by the National Key Research and Development Program of China (2022YFC3401600), the National Natural Science Foundation of China (32171372), the Program A for Outstanding PhD Candidate of Nanjing University (202102A004), the Logistics Research Projects (BWS20J017), and the University of Sydney–China Scholarship Council (USYD-CSC) scholarship (202008320366). We would like to thank Editage (www.editage.cn) for English language editing.

Compliance with ethics guidelines

Wenjing Zai, Yunong Yuan, Lin Kang, Jialong Xu, Yiqiao Hu, Lifeng Kang, and Jinhui Wu declare that they have no competing interests.

Appendix A. Supplementary data

Supplementary data to this article can be found online at https://doi.org/10.1016/j.eng.2023.05.006.

References

[1] Sun BK, Siprashvili Z, Khavari PA. Advances in skin grafting and treatment of cutaneous wounds. Science 2014;346(6212):941–5.
[2] Sen CK, Gordillo GM, Roy S, Kirsner R, Lambert L, Hunt TK, et al. Human skin wounds: a major and snowballing threat to public health and the economy. Wound Repair Regen 2009;17(6):763–71.
[3] Clay L, Stark B, Gunnarsson U, Strigård K. Full-thickness skin graft vs. synthetic mesh in the repair of giant incisional hernia: a randomized controlled multicenter study. Hernia 2018;22(2):325–32.
[4] Winsnes A, Falk P, Gunnarsson U, Strigård K. Full-thickness skin grafts to reinforce the abdominal wall: a cross-sectional histological study comparing intra- and extraperitoneal onlay positions in mice. J Wound Care 2022;31(1):48–55.
[5] Peck MD. Epidemiology of burns throughout the world. Part I: distribution and risk factors. Burns 2011;37(7):1087–100.
[6] Butler KL, Goverman J, Ma H, Fischman A, Yu YM, Bilodeau M, et al. Stem cells and burns: review and therapeutic implications. J Burn Care Res 2010;31(6):874–81.
[7] Andreassi A, Bilenchi R, Biagioli M, D'Aniello C. Classification and pathophysiology of skin grafts. Clin Dermatol 2005;23(4):332–7.
[8] Silva ITS, Menezes HF, Souza Neto VL, Sales JRP, Sousa PAF, et al. Terminological subset of the international classification for nursing practice for patients hospitalized due to burns. Rev Esc Enferm. In press.
[9] Smith MK, Mooney DJ. Hypoxia leads to necrotic hepatocyte death. J Biomed Mater Res A 2007;80(3):520–9.
[10] Malda J, Rouwkema J, Martens DE, Le Comte EP, Kooy FK, Tramper J, et al. Oxygen gradients in tissue-engineered PEGT/PBT cartilaginous constructs: measurement and modeling. Biotechnol Bioeng 2004;86(1):9–18.
[11] Semenza GL. Life with oxygen. Science 2007;318(5847):62–4.
[12] Marks H, Bucknor A, Roussakis E, Nowell N, Kamali P, Cascales JP, et al. A paintable phosphorescent bandage for postoperative tissue oxygen assessment in DIEP flap reconstruction. Sci Adv 2020;6(51):eabd1061.
[13] Lin SJ, Nguyen MD, Chen C, Colakoglu S, Curtis MS, Tobias AM, et al. Tissue oximetry monitoring in microsurgical breast reconstruction decreases flap loss and improves rate of flap salvage. Plast Reconstr Surg 2011;127(3):1080–5.
[14] Al-Waili NS, Butler GJ. Effects of hyperbaric oxygen on inflammatory response to wound and trauma: possible mechanism of action. Sci World J 2006;6:425–41.
[15] Reading SA, Yeomans M, Levesque C. Skin oxygen tension is improved by immersion in oxygen-enriched water. Int J Cosmet Sci 2013;35(6):600–7.
[16] Heyboer 3rd M, Sharma D, Santiago W, McCulloch N. Hyperbaric oxygen therapy: side effects defined and quantified. Adv Wound Care 2017;6(6):210–24.
[17] Chen CY, Wu PW, Hsu MC, Hsieh CJ, Chou MC. Adjunctive hyperbaric oxygen therapy for healing of chronic diabetic foot ulcers. J Wound Ostomy Cont 2017;44(6):536–45.
[18] Dissemond J, Kröger K, Storck M, Risse A, Engels P. Topical oxygen wound therapies for chronic wounds: a review. J Wound Care 2015;24(2):53–4,56–60,62–3.
[19] Gordillo GM, Sen CK. Evidence-based recommendations for the use of topical oxygen therapy in the treatment of lower extremity wounds. Int J Low Extrem Wounds 2009;8(2):105–11.
[20] Tawfick WA, Sultan S. Technical and clinical outcome of topical wound oxygen in comparison to conventional compression dressings in the management of refractory nonhealing venous ulcers. Vasc Endovascular Surg 2013;47(1):30–7.
[21] Chen H, Cheng Y, Tian J, Yang P, Zhang X, Chen Y, et al. Dissolved oxygen from microalgae-gel patch promotes chronic wound healing in diabetes. Sci Adv 2020;6(20):eaba4311.
[22] Ochoa M, Rahimi R, Zhou J, Jiang H, Yoon CK, Maddipatla D, et al. Integrated sensing and delivery of oxygen for next-generation smart wound dressings. Microsyst Nanoeng 2020;6(1):46.
[23] Lewis AS. Eliminating oxygen supply limitations for transplanted microencapsulated islets in the treatment of type 1 diabetes [dissertation]. Cambridge: Massachusetts Institute of Technology; 2008.
[24] Davis SC, Cazzaniga AL, Ricotti C, Zalesky P, Hsu LC, Creech J, et al. Topical oxygen emulsion: a novel wound therapy. Arch Dermatol 2007;143(10):1252–6.
[25] Li J, Zhang YP, Zarei M, Zhu L, Sierra JO, Mertz PM, et al. A topical aqueous oxygen emulsion stimulates granulation tissue formation in a porcine second-degree burn wound. Burns 2015;41(5):1049–57.
[26] Kalidasan V, Yang X, Xiong Z, Li RR, Yao H, Godaba H, et al. Wirelessly operated bioelectronic sutures for the monitoring of deep surgical wounds. Nat Biomed Eng 2021;5(10):1217–27.
[27] Liu M, Zhang Y, Liu K, Zhang G, Mao Y, Chen L, et al. Biomimicking antibacterial opto-electro sensing sutures made of regenerated silk proteins. Adv Mater 2021;33(1):e2004733.
[28] Zhu J, Jin Q, Zhao H, Zhu W, Liu Z, et al. Reactive oxygen species scavenging sutures for enhanced wound sealing and repair. Small struct 2021;2(7):2100002.
[29] Zai W, Kang L, Dong T, Wang H, Yin L, Gan S, et al. *E. coli* membrane vesicles as a catalase carrier for long-term tumor hypoxia relief to enhance radiotherapy. ACS Nano 2021;15(9):15381–94.
[30] Ma Z, Yang Z, Gao Q, Bao G, Valiei A, Yang F, et al. Bioinspired tough gel sheath for robust and versatile surface functionalization. Sci Adv 2021;7(15):eabc3012.
[31] Wang LH, Ernst AU, An D, Datta AK, Epel B, Kotecha M, et al. A bioinspired scaffold for rapid oxygenation of cell encapsulation systems. Nat Commun 2021;12(1):5846.
[32] Farzin A, Hassan S, Teixeira LSM, Gurian M, Crispim JF, Manhas V, et al. Self-oxygenation of tissues orchestrates full-thickness vascularization of living implants. Adv Funct Mater 2021;31(42):2100850.
[33] Ishihara J, Ishihara A, Starke RD, Peghaire CR, Smith KE, McKinnon TAJ, et al. The heparin binding domain of von Willebrand factor binds to growth factors and promotes angiogenesis in wound healing. Blood 2019;133(24):2559–69.
[34] Randi AM, Laffan MA. von Willebrand factor and angiogenesis: basic and applied issues. J Thromb Haemost 2017;15(1):13–20.
[35] Chen KT, Mardini S, Chuang DCC, Lin CH, Cheng MH, Lin YT, et al. Timing of presentation of the first signs of vascular compromise dictates the salvage outcome of free flap transfers. Plast Reconstr Surg 2007;120(1):187–95.
[36] Davis JS. Address of the president: the story of plastic surgery. Ann Surg 1941;113(5):641–56.
[37] Holmdahl V, Stark B, Clay L, Gunnarsson U, Strigård K. Long-term follow-up of full-thickness skin grafting in giant incisional hernia repair: a randomised controlled trial. Hernia 2022;26(2):473–9.
[38] Willemen NGA, Hassan S, Gurian M, Jasso-Salazar MF, Fan K, Wang H, et al. Enzyme-mediated alleviation of peroxide toxicity in self-oxygenating biomaterials. Adv Healthc Mater 2022;11(13):e2102697.
[39] Yuan Y, Han Y, Yap CW, Kochhar JS, Li H, Xiang X, et al. Prediction of drug permeation through microneedled skin by machine learning. Bioeng Transl Med 2023;10512:e10512.
[40] Kudur MH, Pai SB, Sripathi H, Prabhu S. Sutures and suturing techniques in skin closure. Indian J Dermatol Ve 2009;75(4):425–34.